16th World Conference on Earthquake, 16WCEE 2017
Santiago Chile, January 9th to 13th 2017
Paper N° 453
Registration Code: S-B1463243937

DYNAMIC CHARACTERISTICS OF A TWENTY-STORY INSTRUMENTED BUILDING IN ANCHORAGE, ALASKA IDENTIFIED BY SEISMIC INTERFEROMETRY

E. Kalkan[(1)] and W. Wen[(2)]

[(1)] Research Structural Engineer, Earthquake Science Center, U.S. Geological Survey, CA, USA, ekalkan@usgs.gov
[(2)] Lecturer, Key Lab of Structures Dynamics Behavior and Control of the Ministry of Education, Harbin Institute of Technology, Harbin, China, wenweiping@hit.edu.cn

Abstract

Seismic interferometry by deconvolution is used for system identification of a twenty-story steel, moment-resisting frame building (Robert B. Atwood Building) in downtown Anchorage, Alaska. This regular-plan mid-rise structure is instrumented with a 32-channel accelerometer array at ten levels. The impulse response functions (IRFs) are computed based on waveforms recorded from five local and regional earthquakes. The earthquakes occurred from 2005 to 2014 with moment magnitudes between 4.7 and 6.2 over a range of azimuths at epicentral distances of 13.3 to 183 km. The traveling waves, identified in IRFs with a virtual source at the roof are used to estimate the intrinsic attenuation associated with the fundamental modes of the structure, and shear-wave velocity in the building due to linear response. The median shear-wave velocity from the IRFs of five earthquakes is 191 m/s for the east-west (EW), 205 m/s for the north-south (NS), and 176 m/s for the torsional responses. The building's average intrinsic-damping ratio is estimated as 3.7% and 3.4% along the EW and NS directions, respectively. These results are intended to serve as a reference for undamaged condition of the building, which may be used for tracking changes in structural integrity during and after future earthquakes.

Keywords: Seismic interferometry; deconvolution; impulse response function; shear-wave velocity; intrinsic attenuation; instrumentation

1. Introduction

Wave propagation in buildings can be used for tracking the origin and changes in building's stiffness and strength, which are primary goals of structural-health monitoring (SHM). Seismic interferometric techniques, based on cross-correlation, deconvolution and cross coherence are effective to extract Green's functions, which account for wave-propagation between receivers [1], [2]. Among them, deconvolution interferometry has been used commonly for computing shear-wave propagation in buildings. This method considers correlation of motions at different observation points, and changes the boundary condition at the base; thus the structural response can be recovered using impulse response functions (IRFs) with an assumption of no rocking at the foundation level [3], [4]. This method was applied to earthquake shaking [5]-[14] and ambient-vibration data [14]-[16] to retrieve the velocity of traveling shear-waves and intrinsic attenuation in buildings instrumented with accelerometer arrays.

Recently, a nonlinear least square (LSQ) fit algorithm has been used to mimic the analytical IRFs of the equivalent layered shear beam as close as possible to the observed IRFs computed by deconvolution [17], [18]. In this method, the pulses in the IRFs are fitted as a function of time over predefined time windows. In order to maximize the signal-to-noise ratio (SNR) and decrease the influence of reflected pulses from the layer interfaces, the time windows over which the IRFs are fitted are chosen in a way that they enclose only the main lobes of both the acausal and causal direct pulses.

In this study, we applied deconvolution interferometry (henceforth referred to as the direct method) and also nonlinear least-square fit algorithm (henceforth referred as LSQ method) to earthquake-shaking data recorded from an instrumented building to extract the building dynamic characteristics, and monitor the changes in those characteristics over time. The structure selected is a twenty-story steel-moment frame office building (Robert B. Atwood Building) located in Anchorage, Alaska. The U.S. Geological Survey's (USGS) Advanced National Seismic System furnished this building with a 32-channel accelerometer array at ten levels in 2003. The building is a rare example of densely instrumented structure with a square plan. Its structural instrumentation is

accompanied by a free-field station and geotechnical borehole array located in Delaney Park, 180 m away from the building, to measure soft sediment response to earthquake shaking, and to provide input wave-field data for the structure. Fig. 1 shows the photo and map view of Atwood Building and Delaney Park borehole array.

Fig. 1 – Photo showing north façade of twenty-story high Atwood Building next to the Delaney Park geotechnical borehole array (fenced area) in downtown Anchorage, Alaska. Google map insert shows the location of Delaney Park (photo source = E. Kalkan).

Since 2003, more than a dozen earthquakes with moment magnitude (**M**) 4.5 and above have been recorded by the building's accelerometer array. Using earthquake-shaking data, we identify traveling waves in the IRFs with a virtual source at the roof to compute the shear-wave velocity profile of the building and to determine the intrinsic attenuation associated with the fundamental modes of the structure. The shear-wave velocity is a good indicator of nonlinearity as it is directly related to the structural rigidity, and its decrease over time indicates a change in stiffness conceivably initiated by structural damage [3], [7], [12]-[14], [19].

The results of this full-scale case study not only confirm the robustness of deconvolution interferometry for system identification, but also serve as a reference for the undamaged condition of the Atwood Building for tracking changes in its structural integrity during and after future earthquakes.

2. Building Instrumentation and Data

The Atwood Building, located in northwest downtown Anchorage, Alaska is a twenty-story (80.54 m) moment-resisting steel frame office structure with a basement used as a parking garage. The building was designed according to 1979 Uniform Building Code (ICBO, 1979), and constructed in 1980. It has a square footprint of 39.6 m with a square concrete core of 14.6 m. The building's reinforced concrete shallow foundation consists of a 1.52 m thick mat under the center core with a perimeter wall footing connected with grade beams.

The instrumentation consists of a 24 bit IP-based Kinemetrics Granite data logger and an array of 32 accelerometers distributed on ten levels: basement, 1st (ground), 2nd, 7th, 8th, 13th, 14th, 19th, 20th and roof (Fig. 2). Among the sensors, 29 of them are 2g-uniaxial (Kinemetrics ES-U) and one is a tri-axial Force Balance Accelerometer (Kinemetrics ES-T) with 1.25 Volt/g sensitivity. The ES-T (channels 1 through 3) is located at the northwest corner of the basement to measure the three components input ground motion. Two vertically oriented accelerometers (channels 4 and 6) are located on the basement at the southwest and northeast corners to compute the rocking motion. The rest of the 27 accelerometers were placed on nine different floors to measure the building's lateral motions along the EW and NS directions, and to compute its torsional motions. The relative

floor displacements (story drifts) can be computed using the recorded accelerations at the same corners of the building. This accelerometer array records 200 samples-per-second data in real-time; data is stored on a ring-buffer of the data logger. Further details of the building's structural system and site geology can be found in [14].

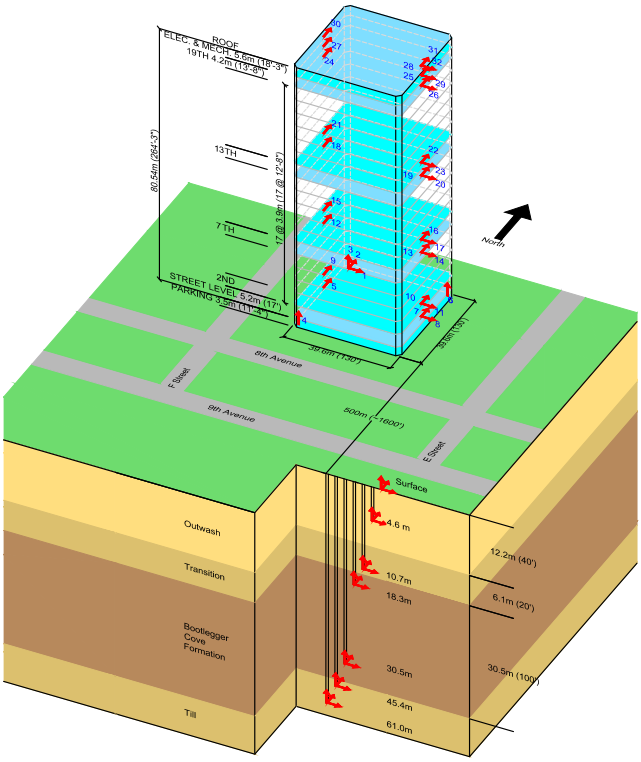

Fig. 2 – Instrumentation layout of the Atwood Building array and nearby Delaney Park borehole array; red arrows indicate sensor orientation; blue numbers indicate sensor IDs. Elevations denote the height of each floor from the ground level. Geologic profile is also shown.

More than a dozen earthquakes with **M**4.5 and above have been recorded with no signs of damage and the authors are not aware of any structural damage since the deployment of the building array. Five earthquakes with **M** between 4.5 and 6.2 were identified for this study based on their proximity to the building and intensity of recordings. The distant small magnitude earthquakes were discarded due to low SNR of their waveforms. The events selected are listed in Table 1 along with distance, depth and epicenter coordinates.

Table 1 – Origin times, magnitudes, epicenter locations of local and regional earthquakes recorded by the Atwood Building accelerometer array in Anchorage, Alaska between 2005 and 2014.

Event No.	Origin time (UTC) (y-m-d; h:m:s)	Moment magnitude	Epicenter Coordinates Lat. (°)	Long. (°)	Depth (km)	Epicentral Distance (km)	Peak Acceleration: Ground	Structure (cm/s^2)
1	2005-04-06; 17:51:36	4.9	61.454	-146.518	17.0	183.0	8.1	13.7
2	2006-07-27; 06:42:37	4.7	61.155	-149.678	36.0	13.3	24.3	41.8
3	2009-06-22; 11:28:05	5.4	61.939	-150.704	64.6	89.4	7.9	18.6
4	2010-09-20; 13:44:02	4.9	61.115	-150.219	45.4	20.7	22.8	38.1
5	2014-09-25; 09:51:17	6.2	61.950	-151.790	102.8	102.1	71.6	147.1

The epicentral locations of those events are depicted on a regional map in Fig. 3; also shown in this map are known active faults in the vicinity of Anchorage. Events selected are 17 to 102.8 km deep. Fig. 4 compares floor horizontal accelerations recorded at the first floor with those at the roof level during the five earthquakes. The largest peak acceleration of 15% g was recorded at the roof level of the building during the 25 September 2014 (**M**6.2) event at epicentral distance of 102.1 km. The waveforms from the first floor amplify as much as 2.8 times from the first floor to the roof level due to the building's response.

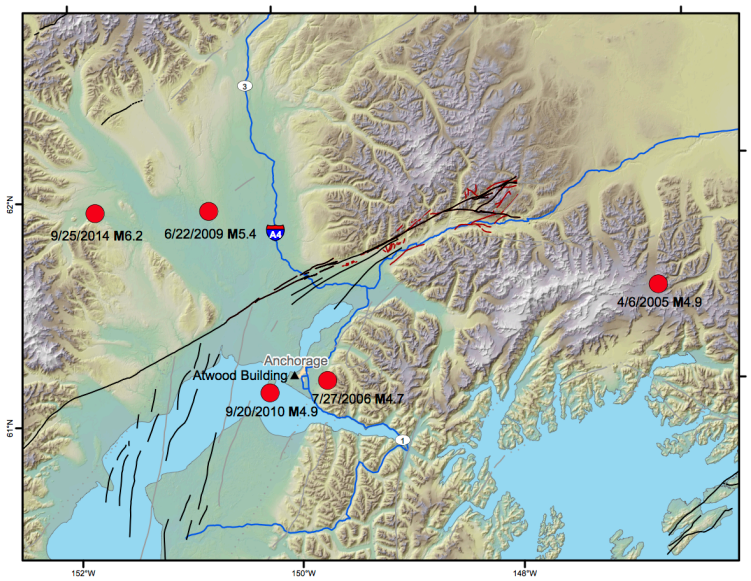

Fig. 3 – Map showing location of the Atwood Building by black triangle (N61.21528° and W149.89296°) and epicenters of selected five earthquakes with circles (summarized in Table 1). Quaternary faults and major highways are indicated in and around Anchorage, Alaska [**M** = moment magnitude].

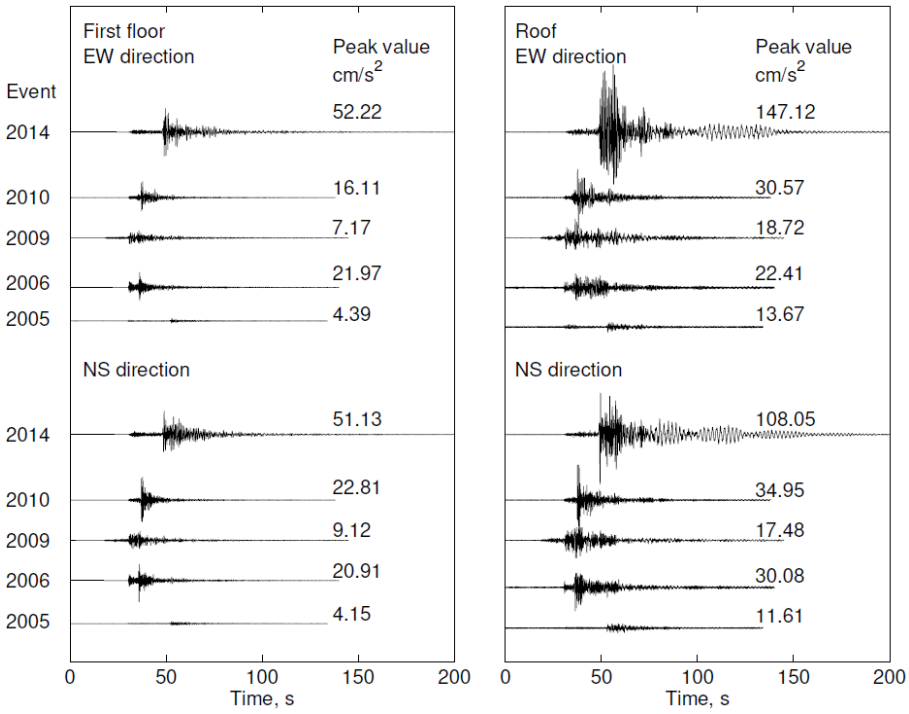

Fig. 4 – Horizontal acceleration waveforms recorded at first-floor and roof levels during five earthquakes summarized in Table 1 [waveforms are not aligned in time].

3. Deconvolution Interferometry

The deconvolution of the response at height $z, u(z)$ by the response at height z_a, $u(z_a)$ is defined as

$$D(z, z_a, \omega) = u(z)/u(z_a) \tag{1}$$

The above equation may become unstable when the denominator approaches zero. Thus, the following regularized format is used as an estimator of deconvolution:

$$D(z, z_a, \omega) = [u(z)u^*(z_a)]/[|u(z_a)|^2 + \varepsilon\langle|u(z_a)|^2\rangle] \tag{2}$$

where superscript "*" denotes the complex conjugate, ε is the regularization parameter (ε=0.01 is used here), and $\langle|u(z_a)|^2\rangle$ is the average power spectrum of $u(z_a)$.

The incoming wave $S(\omega)$ and the reflection coefficient $R(\omega)$ do not present in the analytical expression of deconvolution [5], [11], [14], and thus deconvolution interferometry can remove the influences of $S(\omega)$ and $R(\omega)$. The incoming and reflection waves refer to the traveling waves within the building. The response also depends on the foundation rocking when one considers models with higher degrees of freedom of the base of the building, such as horizontal and rocking motions, for which the response is coupled [3], [21]. Following Eq. (2), the IRFs can be computed. Full derivation of the deconvolution equations is reported in [11], [14].

4. LSQ Multilayer Model Fit

The LSQ method is also used for multilayer model fitting. This algorithm involves fitting of pulses in the IRFs as functions of time, over predefined time windows [18]. The time windows are chosen such that they encompass only the main lobes of both the acausal and causal direct pulses. This is to maximize SNR and decrease the influences of reflected pulses from the layer interfaces. The solution of the LSQ fit is based on Levenberg-Marquardt method [22], [23], which is an iterative approach and relies on initial value of shear-wave velocity for convergence. The initial value of the shear-wave velocity is estimated as the ratio of distance between layers of shear-beam and time lag between pulses computed from the direct method. The main advantages of this method over the direct method are that it uses information about the pulse amplitudes and it is not limited by the postulation of ray theory that variation of material properties across the model is smooth [19].

5. Results

Both direct and LSQ methods were applied to the horizontal components of waveforms recorded in the building from five earthquakes listed in Table 1. The structural responses $u(z)$ from instrumented floors were deconvolved by the structural response measured at the roof $u(H)$ for two orthogonal directions separately. Full lengths of the waveforms, shown in Fig. 4, were used because the building's response remained linear-elastic. The IRFs (deconvolved waveforms) were bandpass filtered with corner frequencies of 0.2 and 8.0 Hz using a second order acausal (zero phase-shift) Butterworth filter to accentuate at least three fundamental modes in EW, NS and torsional responses. Then, the LSQ method was applied. Fig. 5 illustrates the IRFs computed by both methods.

The simplicity of the IRFs suggests that the wave propagation is essentially one-dimensional for the frequency envelope chosen. The IRFs contain energy in the acausal part (no phase shift) because there is no physical source at the roof. The building response at height z deconvolved by the response at the roof is the summation of the two attenuated waves traveling upward and downward. For negative time, upward-going waves are present that reflect at the roof at t = 0 s. If the waveforms are deconvolved with the waveform at the basement, they will not display acausal arrivals, and resultants IRFs will be more complicated. This is because the reflected arrivals are present in the basement record.

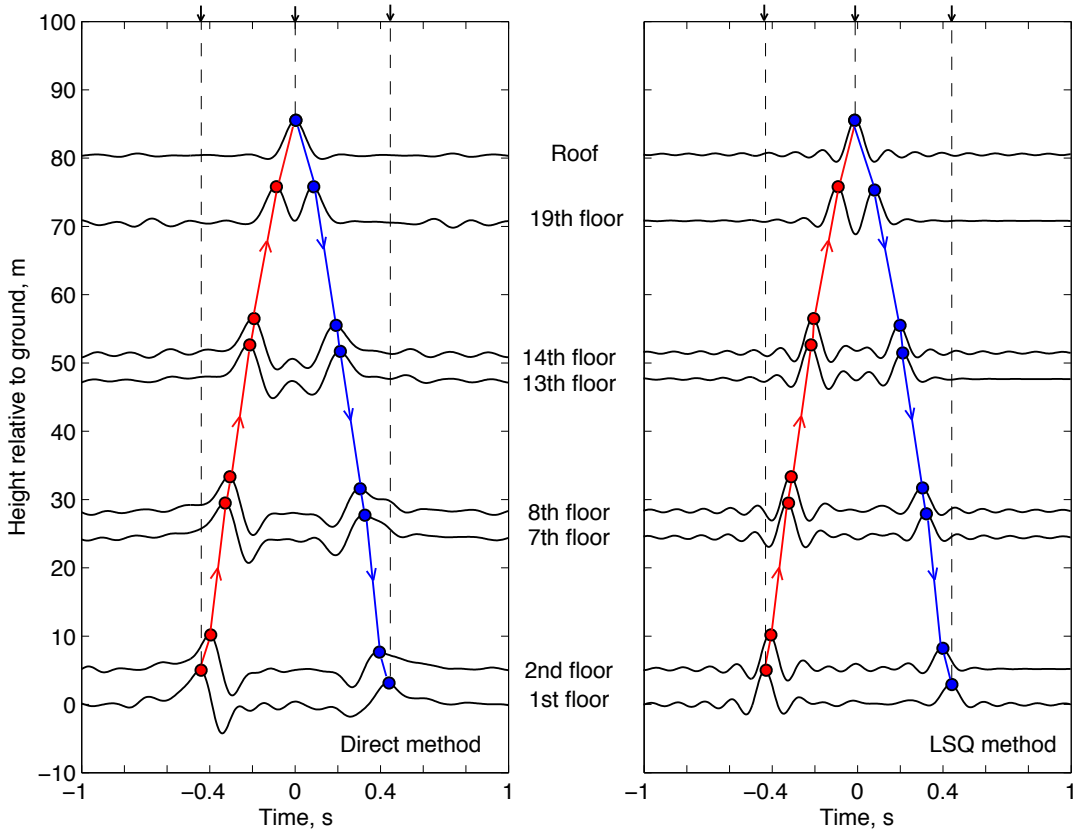

Fig. 5 – Impulse response functions, calculated from the 25 September 2014 (**M**6.2) earthquake east-west-direction acceleration time series, are plotted as positive and negative amplitudes for each instrumented floor over time using direct method (left panel) and LSQ method (right panel). Virtual source is at the roof; thus the deconvolved waveforms are acausal. Arrows denote the upward and downward traveling waves. Vertical arrows are used to estimate two-way average travel times for upward and downward traveling waves. Frequency range of the waveforms is 0.2 – 8.0 Hz.

5.1 Shear-wave Velocity

The shear-wave velocity of traveling waves ($V_{S,n}$) for the n^{th} layer between two receivers is derived based on the time lag τ between peaks of IRFs and the travel distance following ray theory, which disregards wave scattering ($V_{S,n} = h/\tau$, where h is the distance in meter). As shown in Fig. 6, we model the building as a simple 4-layer elastic layered shear-beam according to the receiver locations; the layers are numbered from top to bottom. This model, appropriate for moment-frame structures over certain frequency bands [18], is supported by a half-space and excited by vertically incident plane shear waves without foundation rocking. The layers, consisting of groups of floors, are assumed to be homogenous, isotropic, perfectly bonded to each other. The tilt motions, computed from measurements of multiple vertical accelerometers at the basement of the building, do not reveal any foundation rocking.

Fig. 7 shows the shear-wave velocity profiles computed by direct and LSQ methods. The shear-wave velocities along the building height gradually decrease from top to base; this is attributed to the upper portion of the building being less stiff than the lower portion because the section size of structural components reduces towards the upper floors. The variation of velocities between different earthquakes is comparable.

Based on the results of IRFs identified by both methods, the average shear-wave velocity of the entire building is determined. An example computation is portrayed in Fig. 8, where the square and circular marks correspond to the peaks in the IRFs as shown in Fig. 5. The travel distance is measured relative to the position of

the virtual source (roof). The negative travel distance is for upward traveling wave. A straight line is fitted to the distance and time pairs identified from the upward and downward traveling waves using least squares with the Levenberg-Marquardt method.

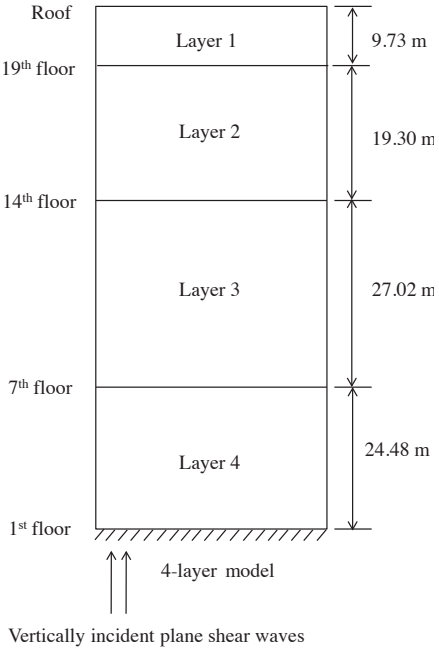

Fig. 6 – Correspondence between layers and floor numbers of 4-layer shear-beam model used to calculate the average shear-wave velocity of the Atwood Building; heights of each layer are depicted.

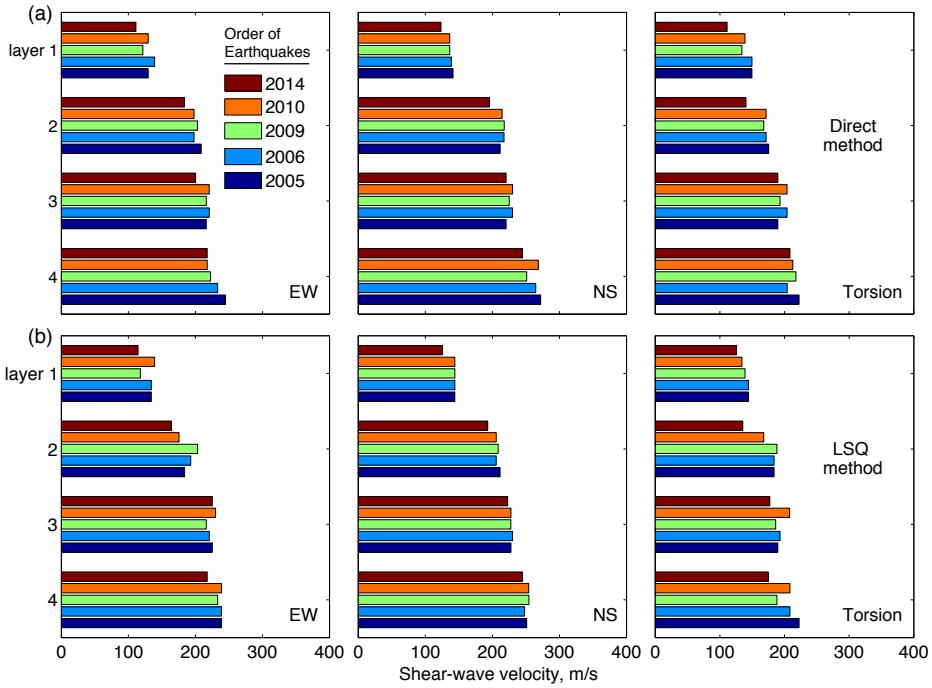

Fig. 7 – Shear-wave velocity profiles of the Atwood Building for east-west (EW), north-south (NS) and torsional responses considering 4-layer shear-beam model and five earthquakes (color coded) based on (a) direct method (top panels) and (b) LSQ method (bottom panels); [Layer 1 = upper floors; Layer 3 = lower floors; earthquakes are in descending order according to occurrence year at each layer].

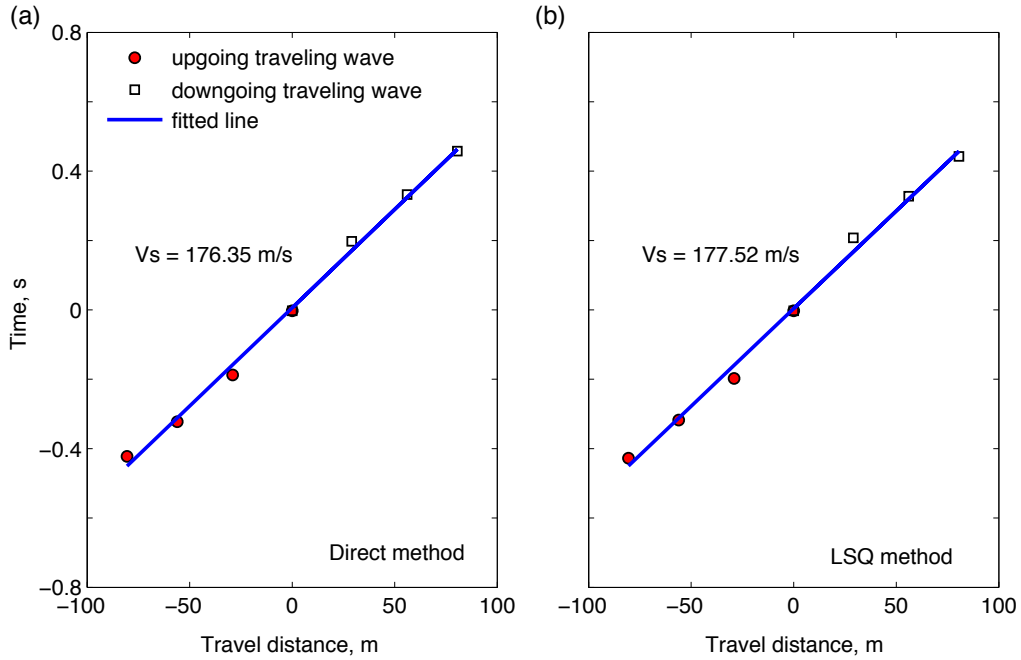

Fig. 8 – Shear-wave velocity of the entire building calculated based on 4-layer shear-beam model using the peaks of impulse response function amplitudes obtained from (a) direct and (b) LSQ methods. Data correspond to the east-west direction waveforms of the 25 September 2014 (**M**6.2) earthquake (Event No. 5).

The aforementioned two methods were applied to the remaining four earthquake data and the median and standard deviation results are summarized in Table 2. The average shear-wave velocities along the EW direction is in general 10% less than those along the NS direction because the stiffness of the building along the NS direction is slightly larger than that along the EW direction [14]. The shear-wave velocity is found to be lowest for the 2014 event (Event No. 5) that shook the building the strongest. The results of LSQ method are slightly less than those of direct method, and the differences are generally within 5%.

Table 2. Average shear-wave velocity of the Atwood Building based on direct and LSQ methods using 4-layer shear-beam model; unit is m/s. See Table 1 for event information.

		Event No.						
	Direction	1	2	3	4	5	Median	Standard deviation
Direct method	East-West	198	198	191	193	176	191	9.0
	North-South	207	210	206	209	193	205	6.9
	Torsion	183	183	177	182	158	176	10.7
LSQ method	East-West	194	196	191	194	178	190	7.3
	North-South	208	207	207	207	194	204	5.9
	Torsion	184	183	178	180	153	175	12.9

5.2 Intrinsic Attenuation

During wave propagation, the energy loss induced by intrinsic damping can be represented by the following attenuation equation [24]:

$$A_s(f) = \exp\left(-\pi \cdot f \cdot \frac{\tau}{Q}\right) \tag{3}$$

where $A_s(f)$ is the reduction in the amplitude of a sinusoidal wave frequency f when it travels a distance of travel time τ, and Q is the quality factor. The damping ratio ξ is defined by Q as $\xi = \frac{1}{2Q}$.

In order to evaluate the intrinsic attenuation in structures, previous studies [5], [10], [11], [15] used Eq. (3) in conjunction with the IRFs; the same approach is adopted here since it separates intrinsic attenuation and radiation damping. First, the recordings at different floors were deconvolved with the recordings at the first floor to generate causal IRFs. The IRFs are filtered around the resonant frequencies using a second order Butterworth bandpass filter, and the envelope is plotted. The natural logarithms of the envelopes of the bandpass-filtered waveforms corresponding to the 25 September 2014 (**M**6.2) earthquake are shown in Fig. 9. In order to separate the curves at different heights, the natural logarithm of the envelope is added with the floor number. Only the slopes of the curves depend on the attenuation of the waves; thus the offset has no influence on the results. The slopes of the curves, which are similar at different floors, were computed in the least square sense between t_1 and t_2 with the Levenberg-Marquardt method. The decay of natural logarithm of the envelope follows the rule between t_1 and t_2, defined by Eq. (3), while the exponential decay is not valid for the later times [5]. The values of t_1 and t_2 are determined by inspecting the deconvolved waveforms of different earthquakes. The slope of the fitted line is equal to $-\pi f/Q$. By using different instrumented floors, one may obtain uncertainty measurements. The consistency of Q values for each instrumented floor indicates the measurement accuracy. The mean slope at different layers (which is generally consistent at different floors) and the first mode frequencies identified with the wave velocity were used to compute the average Q and ξ. The fundamental frequencies of the structure were computed from the complex mode indicator function explained in detail in [14].

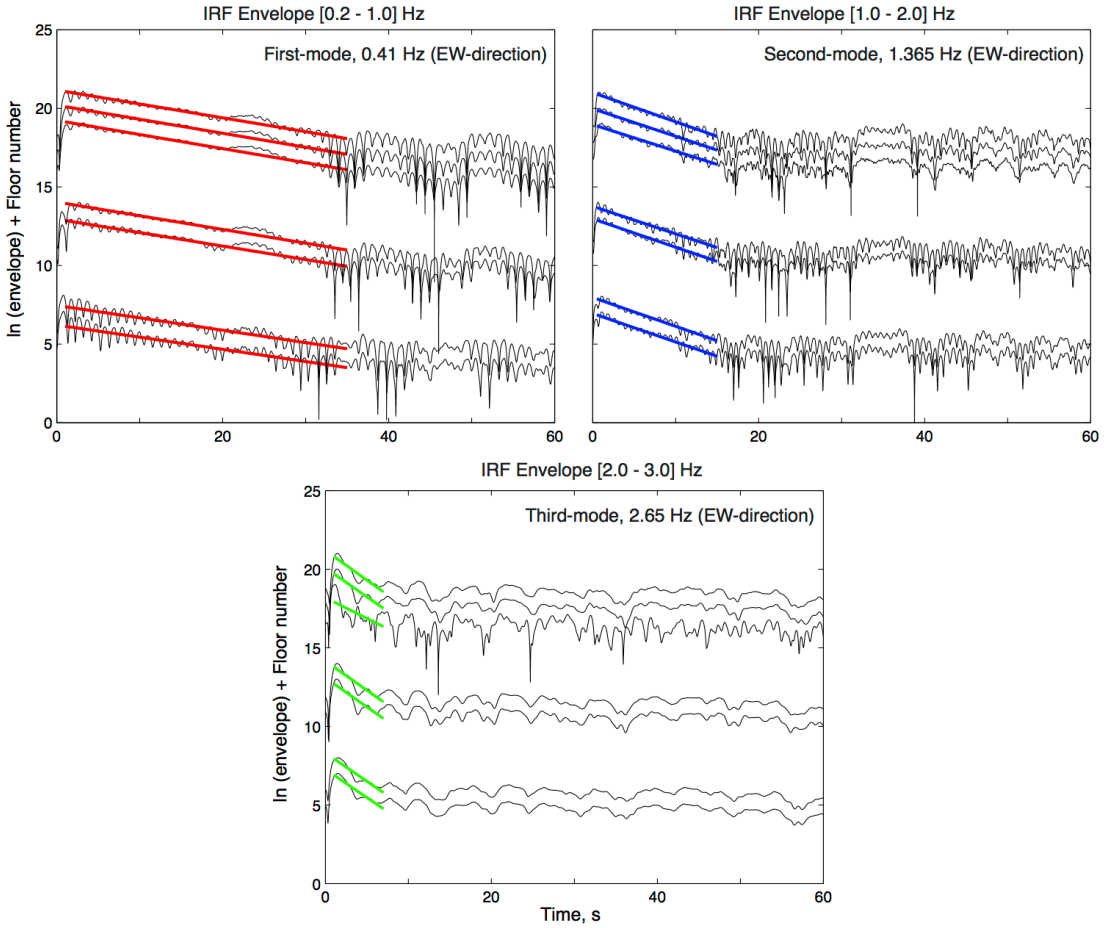

Fig. 9 – Impulse response function (IRF) envelopes in natural logarithmic scale for the first-three fundamental modes in the east-west (EW) direction. The data correspond to the 25 September 2014 (**M**6.2) earthquake.

Table 3 summarizes the results for all events. The damping in the EW direction is slightly larger than that in the north-south direction. The dispersion of the damping ratio is moderate with a coefficient of variation of 16%. The average damping ratio is found to be 3.7% and 3.4% along the east-west and north-south directions for the fundamental modes. We interpret the damping as that of the structure because rocking for the building is insignificant.

Table 3. Mean slope of different layers, quality factor Q, and intrinsic-damping ratio ξ (in percentage) computed for different earthquakes.

Event	East-West			North-South		
No.	Slope	Q	ξ (%)	Slope	Q	ξ(%)
1	-0.11	13.6	3.7	-0.11	16.2	3.1
2	-0.10	14.7	3.4	-0.10	16.3	3.1
3	-0.12	12.1	4.1	-0.14	12.3	4.1
4	-0.11	13.1	3.8	-0.12	13.1	3.8
5	-0.09	15.1	3.3	-0.09	16.2	3.1
Average		13.7	3.7		14.8	3.4

6. Conclusions

Deconvolution interferometry (direct method) and LSQ multilayer fit method (LSQ method) are applied to the waveform data recorded in a twenty-story structure in Anchorage Alaska to retrieve vertically propagating shear waves in the building. This structure (Robert B. Atwood Building) is an excellent example of mid-rise symmetric-plan steel, moment-resisting frame office building, typical of urban settings. The waveform data from a 32-channel accelerometer array include accelerations observed from five small and moderate, local and regional earthquakes. The data were used to compute the impulse response functions (IRFs), which led to estimation of velocities of traveling waves and intrinsic attenuation. This work presents a backbone dataset of system-identification measurements for the undamaged condition of this building, which may then be used for tracking changes in structural integrity during and after future earthquakes. The key findings of this study are as follows:

1. The simplicity and similarity of the IRFs from different earthquakes suggest that a one-dimensional shear-beam is a reasonable model to quantify the building's linear-elastic dynamic properties. This conclusion is supported by the vertically propagating shear waves, which are found to be non-dispersive due to insignificant foundation rocking observed during the earthquakes. If significant rocking motion existed, it would not only affect the damping due to the soil-structure interaction but also result in dispersive response of deconvolved wavefields in the building due to coupling of horizontal and rocking motions.

2. The estimated median shear-wave velocity from IRFs of five earthquakes is 191 m/s for the east-west (EW), 205 m/s for the north-south (NS), and 176 m/s for the torsional responses according to the direct method. The shear-wave velocity is found to be lower for the 2014 event that shook the building stronger. We interpret the change in shear-waves (and frequencies) that we observe during the stronger event to be due to opening and closing of gaps between non-structural and structural components. The shear-wave velocity results obtained by direct deconvolution are similar to those obtained using the LSQ method. The difference between the direct and LSQ methods is within 5%.

3. The damping ratio identified by the deconvolution interferometry is consistent for five earthquakes. The average intrinsic-damping ratio is found to be 3.5% in the translational directions. We interpret the damping as that of the structure because rocking for the building was not significant for these earthquakes.

7. Data and Resources

Instruments of the National Strong Motion Network of USGS collected recordings used in this study. The records from the 22 June 2009 (**M**5.4) and 25 September 2014 (**M**6.2) earthquakes can be downloaded from *http://www.strongmotioncenter.org/* (accessed May, 2016). The records from the 06 April 2005 (**M**4.9), 27 July 2006 (**M**4.7) and 20 September 2010 (**M**4.9) earthquakes are available from the National Strong Motion Project (GS-G-WR_ESC_NSMP@usgs.gov) upon request. Fig. 2 is modified from *http://nees.ucsb.edu/facilities/atwood-building-anchorage* (accessed May, 2016).

8. Acknowledgements

We would like to thank Art Frankel, Rob Graves, Maria Todorovska, Nori Nakata and Brad Aagaard for their reviews and offering useful comments and suggestions, which helped to improve the technical quality and presentation of our work. Special thanks are extended to Christopher Stephens for providing the waveform data, Luke Blair for preparing the regional earthquake fault maps, Shahneam Reza for drafting the sensor lay out, Suzanne Hecker for final editing. We also thank Joe Fletcher, and Nori Nakata for technical discussions and sharing their computer codes, which we modified significantly for this study. Last but not least, we would like to thank USGS's National Strong Motion Network technicians James Smith and Jason De Christofaro for keeping the Atwood Building seismic array up and running. China Scholarship Council provided the financial support for Weiping Wen.

9. References

[1] Snieder R, Miyazawa M, Slob E, Vasconcelos I, Wapenaar K (2009): A comparison of strategies for seismic interferometry, *Surveys in Geophysics*, **30**(4-5), 503-523.

[2] Wapenaar K, Draganov D, Snieder R, Campman X, Verdel A (2010): Tutorial on seismic interferometry: Part 1-basic principles and applications. *Geophysics*, **75**(5), A195–A209.

[3] Todorovska MI (2009): Seismic interferometry of a soil-structure interaction model with coupled horizontal and rocking response, *Bulletin of the Seismological Society*, **99**(2A), 611–625.

[4] Rahmani M, Ebrahimian M, Todorovska MI (2015): Wave dispersion in high-rise buildings due to soil-structure interaction. *Earthquake Engineering and Structural Dynamics*, **44**, 317-323.

[5] Snieder R, Şafak E (2006): Extracting the building response using seismic interferometry: theory and application to the Millikan library in Pasadena, California. *Bulletin of the Seismological Society*, **96**(2), 586–598.

[6] Kohler MD, Heaton TH, Bradford SC (2007): Propagating waves in the steel, moment-frame factor building recorded during earthquakes, *Bulletin of the Seismological Society*, **97**(4), 1334–1345.

[7] Todorovska MI, Trifunac MD (2008): Impulse response analysis of the Van Nuys 7-story hotel during 11 earthquakes and earthquake damage detection. *Structural Control and Health Monitoring*, **15**, 90-116.

[8] Picozzi M, Parolai S, Mucciarelli M, Milkereit C, Bindi D, Ditommaso R, Vona M, Gallipoli MR, Zschau J (2011): Interferometric analysis of strong ground motion for structural health monitoring: the example of the L'Aquila, Italy, seismic sequence of 2009. *Bulletin of the Seismological Society*, **101**(2), 635-651.

[9] Picozzi M (2012): An attempt of real-time structural response assessment by an interferometric approach: a tailor-made earthquake early warning for buildings. *Soil Dynamics and Earthquake Engineering*, **38,** 109-118.

[10] Newton C, Snieder R (2012): Estimating intrinsic attenuation of a building using deconvolution interferometry and time reversal. *Bulletin of the Seismological Society*, **102**(5), 2200-2208.

[11] Nakata N, Snieder R, Kuroda S, Ito S, Aizawa T, Kunimi T (2013): Monitoring a building using deconvolution interferometry. I: earthquake-data analysis. *Bulletin of the Seismological Society*, **103**(3), 1662-1678.

[12] Ulusoy HS, Kalkan E, Banga K (2013): Real-time seismic monitoring of Veterans Affairs hospital buildings. *Proceedings of the SPIE Smart Structures Conference*: San Diego, CA.

[13] Nakata N, Tanaka W, Oda Y (2015): Damage detection of a building caused by the 2011 Tohoku-Oki earthquake with seismic Interferometry. *Bulletin of the Seismological Society*, **105**, 2411-2419.

[14] Wen W, Kalkan E (2016): System identification based on deconvolution and cross-correlation—An application to a twenty-story instrumented building in Anchorage, Alaska. *Bulletin of Seismological Society of America*, (in-press).

[15] Prieto GA, Lawrence JF, Chung AI, Kohler MD (2010): Impulse response of civil structures from ambient noise analysis. *Bulletin of the Seismological Society*, **100**(5A), 2322-2328.

[16] Nakata N, Snieder R (2014): Monitoring a building using deconvolution interferometry. II: ambient-vibration analysis. *Bulletin of the Seismological Society*, **104**(1), 204-213.

[17] Todorovska MI, Rahmani M (2012): Recent advances in wave travel time based methodology for structural health monitoring and early earthquake damage detection in buildings. *Proceedings of the 15th World Conference on Earthquake Engineering*, 24-28.

[18] Rahmani M, Todorovska MI (2013): 1D system identification of buildings from earthquake response by seismic interferometry with waveform inversion of impulse responses-method and application to Millikan Library. *Soil Dynamics and Earthquake Engineering*, **47**, 157-174.

[19] Todorovska M. I., and M. Rahmani (2013). System identification of buildings by wave travel time analysis and layered shear beam models—Spatial resolution and accuracy, *Struct. Control Health Monit*. **20**, 686-702.

[20] Kawakami H, Oyunchimeg M (2004): Normalized input-output minimization analysis of earthquake wave propagation in damaged and undamaged buildings. *13th World Conference on Earthquake Engineering,* Vancouver, B.C., Canada, August 1-6, Paper No. 3170.

[21] Rahmani M, Ebrahimian M, Todorovska MI (2015): Time-wave velocity analysis for early earthquake damage detection in buildings: application to a damaged full-scale RC building. *Earthquake Engineering and Structural Dynamics*, **44**(4), 619-636.

[22] Levenberg K (1944): A method for the solution of certain non-linear problems in least squares, *Quart. J. Appl. Maths*. II, **2**, 164–168.

[23] Marquardt DW (1963): An Algorithm for Least-Squares Estimation of Nonlinear Parameters, *SIAM Journal on Applied Mathematics,* **11**(2), 431–441.

[24] Aki K, Richards P.G. (1980): Quantitative seismology: theory and methods, Vol. I, W. H. Freeman and Co., San Francisco.